HPLC-DAD Profiling and Molecular Docking Insights into *Lantana camara* L. Flower Extract from Northwestern Algeria: Verbascoside and Luteolin as Potent Inhibitors of Human Pancreatic α-Amylase.

Bachir Bourroubey

bbmosta2911@yahoo.fr

Mustapha Stambouli University of Mascara, Algeria https://orcid.org/0009-0005-8432-2799

Boumediene Meddah

Mustapha Stambouli University of Mascara, Algeria

Research Article

Keywords: Lantana camara L., Human pancreatic α-amylase, RP-HPLC-DAD, Molecular docking, Luteolin, Verbascoside

Posted Date: July 13th, 2026

DOI: https://doi.org/10.21203/rs.3.rs-10309602/v1

Additional Declarations: The authors declare no competing interests.

Abstract

This study evaluates the anti-diabetic potential of *Lantana camara* L. flowers from Mesra (Mostaganem, Northwestern Algeria). Phytochemical profiling via RP-HPLC-DAD revealed a unique regional chemotype rich in the phenylethanoid glycoside Verbascoside (15.61%, t_R = 8.561 min) and the flavone Luteolin (14.12%, t_R = 18.161 min). This accumulation of specialized secondary metabolites underscores the impact of localized geoclimatic pressures, which upregulate protective phenylpropanoid and core flavonoid pathways.

To elucidate the atomistic mechanisms driving enzyme inhibition, automated molecular docking simulations were executed against human pancreatic α-amylase (HPA, PDB ID: 1HNY) using the Lamarckian Genetic Algorithm. The computational trajectories exposed critical thermodynamic and entropic boundaries governing ligand-receptor affinity. While the standard drug acarbose and the native heteroside Verbascoside established extensive non-covalent contacts, their high molecular flexibility (26 and 20 rotatable bonds, respectively) imposed severe empirical torsional entropy penalties (+ 7.76 kcal/mol and + 5.97 kcal/mol), causing scattered spatial configurations and reduced net binding affinities.

Conversely, the compact, planar flavone matrix of Luteolin bypassed these entropic limitations due to its minimal degrees of freedom (5 rotatable bonds). This reduced conformational entropy penalty (+ 1.49 kcal/mol) allowed Luteolin to converge into a highly focused spatial family (Cluster 2, representing 70% of the statistical ensemble) directly within the deep catalytic cleft. Atomistic parsing demonstrated that this structural rigidity enables precise competitive inhibition, anchoring short-distance hydrogen bonds and close-range π- π stacking networks directly against the conserved catalytic triad (Asp197, Glu233, and Asp300). Consequently, the rigid Luteolin scaffold represents a viable lead compound for managing postprandial hyperglycemia in Type 2 Diabetes Mellitus.

1. Introduction

The global escalation of metabolic disorders, particularly Type 2 Diabetes Mellitus (T2DM), represents one of the most critical therapeutic challenges of the 21st century (International Diabetes Federation, 2021). T2DM is characterized by chronic postprandial hyperglycemia, a condition primarily driven by the rapid enzymatic hydrolysis of dietary carbohydrates in the digestive tract. Human pancreatic α-amylase (EC 3.2.1.1) plays a key role in this metabolic pathway, catalyzing the initial cleavage of endo-α-(1,4)-glucosidic linkages in starch and glycogen into oligosaccharides, which are subsequently converted to glucose by α glucosidases (Tarling et al. 2015). Consequently, the targeted inhibition of pancreatic α-amylase constitutes a primary and well-established clinical strategy to suppress postprandial glucose excursions and manage glycemic loads (Li et al. 2022). While synthetic enzyme inhibitors, most notably acarbose, are widely prescribed in clinical practice, their long-term therapeutic utility is frequently compromised. The systemic retention and non-specific carbohydrate fermentation resulting from heavy synthetic inhibition often induce severe gastrointestinal side effects, including abdominal distension,

flatulence, and diarrhea (Jomova et al. 2025). This clinical limitation has catalyzed a paradigm shift toward the exploration of plant-derived secondary metabolites as safer, bio-compatible alternatives capable of providing balanced enzymatic inhibition with minimized cytotoxic profiles (Kumar at al. 2011).

Among the diverse botanical taxa investigated for their therapeutic potential, *Lantana camara* L. (*Verbenaceae*) has emerged as a prolific source of bioactive scaffolding. Historically integrated into empirical medicine across tropical and subtropical regions, this resilient shrub exhibits a complex phytochemical matrix dense with terpenoids, phenylpropanoids, and flavonoids (He et al. 2024). Crucially, the phytochemical expression and quantitative yield of these secondary metabolites are profoundly dictated by geoclimatic and environmental stressors. The semi-arid and Mediterranean bioclimatic zones of Northwestern Algeria subject local flora to distinct oxidative and thermal pressures (Naviglio et al. 2023; Travis et al. 2026). This specific microenvironment triggers unique adaptive metabolic pathways in *Lantana camara* L., potentially altering its polyphenolic profile and enhancing the enzymatic inhibitory potential of its floral extracts compared to populations studied in other geographical cohorts.

Modern drug discovery increasingly relies on the integration of high-resolution analytical chemistry with computational biochemistry to accelerate the identification of lead compounds. High-Performance Liquid Chromatography (HPLC) coupled with Diode Array Detection (DAD) at targeted wavelengths, such as 300 nm, allows for the precise, reproducible profiling of specialized phenolics (Grosso et al. 2015). Concurrently, in silico molecular docking simulations provide a rigorous, atomistic understanding of ligand protein topologies (Kitchen et al. 2004). By modeling the thermodynamic binding affinities and non-covalent structural interactions within the highly conserved catalytic triad of human pancreatic α-amylase (consisting of Asp197, Glu233, and Asp300), computational modeling bridges the gap between crude botanical screening and targeted molecular therapeutics (Brayer et al. 1995).

Among the structurally diverse constituents identified within the genus, the phenylethanoid glycoside Verbascoside (acteoside) and the flavone Luteolin stand out as compelling candidates for targeted enzymatic modulation. Verbascoside offers an expansive, hydroxyl-rich architecture capable of extensive electrostatic networks (Alipieva et al. 2014), while Luteolin presents a rigid, planar flavone core highly optimized for hydrophobic stacking within deep enzymatic pockets (Tadera et al. 2006). Despite scattered literature on the crude biological assays of the species, a precise comparative structural evaluation focusing on these two specific scaffolds derived explicitly from Algerian biotypes against the human lineage of α amylase has not been systematically established.

This study was designed to address this knowledge gap through a dual experimental and computational framework. Herein, we report the targeted methanolic maceration and quantitative HPLC DAD profiling (at 300 nm) of *Lantana camara* L. flowers harvested from Northwestern Algeria. Furthermore, we deploy rigorous molecular docking simulations to elucidate the competitive binding dynamics, free energy landscapes, and structural interactions of isolated Verbascoside and Luteolin within the active site of human pancreatic α-amylase, directly benchmarking their efficacy against the clinical standard,

acarbose. This work establishes a clear mechanistic rationale for leveraging Algerian *Lantana camara* L. chemotypes as high-affinity, structurally optimized matrices for next-generation antidiabetic drug design.

2. Materials and Methods

2.1. Plant Material Collection and Botanical Authentication

Fresh and healthy flowers of *Lantana camara* L. were harvested during the peak flowering stage in May 2025 from the region of Mesra, located in the Mostaganem province of Northwestern Algeria. The geographical coordinates of the collection site were precisely mapped using Google Maps, corresponding to latitude 35°52'12" N and longitude 0°11'24" E (Fig. 01). The botanical identification and authentication of the plant material were performed based on standard taxonomic keys. A voucher specimen was deposited in the institutional herbarium for future reference. The collected floral samples were meticulously washed with distilled water to remove surface debris, shade-dried at room temperature (25 ± 2 C°) until achieving a constant weight, and subsequently pulverized into a fine, homogeneous powder using a laboratory mechanical grinder. The powder was stored in airtight, amber glass containers at 4°C to prevent phytochemical degradation prior to extraction (Yeasmen and Orsat, 2024).

2.2. Preparation of Methanolic Extract (Maceration)

The extraction of specialized secondary metabolites from the dried flowers was performed via classical solid-liquid maceration, an optimized technique for preserving thermolabile polyphenolic complexes (Naviglio et al. 2023; Travis et al. 2026). Briefly, a 50 g aliquot of the pulverized floral powder was immersed in 500 mL of analytical grade methanol (99.8%, Sigma Aldrich) at a strict 1:10 (w/v) solid to solvent ratio. The mixture was maintained in dark, securely sealed Erlenmeyer flasks at ambient room temperature for 72 hours under continuous, periodic agitation using an orbital shaker (120 rpm). Following the maceration period, the slurry was initially filtered through double layered muslin cloth, followed by clarification through Whatman No. 1 filter paper to remove fine particulate matter. The resulting filtrate was concentrated under reduced pressure using a rotary evaporator (Büchi R-210, Switzerland) at a controlled water bath temperature of 40°C to prevent the thermal artifacts of phenolics. The crude semi-solid methanolic extract was completely desiccated, weighed to calculate the total extraction yield, and preserved in light shielded vials at -20°C for subsequent analytical profiling (Chen et al. 2024).

2.3. HPLC-DAD Phytochemical Profiling and Quantification

The qualitative screening and quantitative monitoring of Verbascoside and Luteolin within the *L. camara* floral extract were conducted using a High-Performance Liquid Chromatography (HPLC) system equipped with a Diode Array Detector (DAD). Chromatographic separation was achieved on a reversed-phase C18 analytical column (250 mm X 4.6 mm, particle size 5 µm) maintained at a constant column temperature of 30°C (Grosso et al. 2015). The mobile phase comprised a binary solvent system

consisting of 0.1% (v/v) formic acid in ultra-pure water (Phase A) and 100% HPLC-grade acetonitrile (Phase B). The elution was performed under an optimized linear gradient program at a constant flow rate of 1.0 mL/min (Alves et al. 2023; Balkrishna et al., 2025).

Prior to injection, the crude methanolic extract was re-dissolved in HPLC-grade methanol and passed through a 0.45 µm polytetrafluoroethylene (PTFE) syringe filter. The injection volume was set to 20 µL. Photodiode array detection was continuously monitored across a multi-wavelength spectrum, with the specific target acquisition fixed at 300 nm, which represents the optimal UV absorption maximum for the simultaneous resolution and structural tracking of both the planar flavone architecture of Luteolin and the phenylethanoid glycoside framework of Verbascoside. Phenolic constituents were identified by rigorously comparing their retention times (t_R) and UV-visible spectral characteristics with those of reference standards. Quantification was accurately extrapolated using external standard calibration curves established for both targeted targets (Alves et al. 2023; Balkrishna et al., 2025).

2.4. In Silico Molecular Docking Simulations

2.4.1. Macromolecule Preparation

The three-dimensional (Fig. 02) crystal structural coordinates of human pancreatic α-amylase (HPA) were retrieved directly from the RCSB Protein Data Bank (PDB ID: 1HNY), resolved at high resolution (Brayer et al. 1995). The protein structure was cleaned and processed within the molecular modeling interface. All crystallographic water molecules, non-functional heteroatoms, and co-crystallized solvent matrices were systematically deleted. As explicitly required for high-fidelity binding simulation environments, the Pyrrolidone Carboxylic Acid (PCA1) residue situated at the N-terminus was structurally retained within the 1HNY enzyme matrix to preserve the native integrity of the protein fold. Missing hydrogen atoms were added, proper atom types were assigned, and Gasteiger-Marsili empirical atomic partial charges were computed. The macromolecule was subjected to a localized energy minimization protocol using the AMBER force field to eliminate steric clashes before running the docking trials.

2.4.2. Ligand Architecture and Optimization

The chemical structures of the identified botanical ligands (Fig. 03), Verbascoside (CID: 5281800) and Luteolin (CID: 5280445), alongside the clinical standard reference drug acarbose (CID: 444305), were obtained from the PubChem database in structural data format (SDF). The configurations were structurally optimized by implementing a comprehensive MMFF94 force field energy minimization protocol within the Avogadro software package to reach the lowest possible structural potential energy. Geometry optimized ligand configurations were subsequently converted to the standard PDBQT format within AutoDock Tools (ADT 1.5.6), ensuring all rotatable bonds were correctly initialized to model ligand flexibility during binding.

2.4.3. Docking Parameterization and Execution

Molecular docking simulations were executed using the AutoDock 4.2.6 program suite, employing the Lamarckian Genetic Algorithm (LGA) to explore the conformational space of the inhibitors within the binding site (Kitchen at al. 2004; Quan et al. 2022; Peanlikhit et al. 2024). To capture targeted interactions with the established active site of human pancreatic α-amylase, a three-dimensional grid box was centered on the catalytic pocket encompassing the key catalytic residues: Asp197, Glu233, and Asp300 (Tarling at al. 2015; Quan et al. 2022; Peanlikhit et al. 2024). The grid box dimensions were optimized with grid spacing configured at 0.375 Å. The LGA search parameters were set to 10 independent docking runs for each compound, with an initial population size of 150 individuals and a maximum number of energy evaluations capped at $2.5 * 10^6$ cycles. The resulting structural conformations were clustered based on an all-atom root-mean-square deviation (RMSD) tolerance of 2.0 Å. The lowest binding free energy (ΔG, kcal/mol) and the respective calculated inhibition constants (Ki) from the most populated cluster were selected for detailed thermodynamic analysis. Visual parsing of non-covalent interactions, hydrogen bonding distances, and hydrophobic pocket configurations was executed using PyMOL and Discovery Studio Visualizer (Quan et al. 2022; Peanlikhit et al. 2024).

3. Results and Discussion

3.1. Chromatographic Characterization and Targeted Quantification

The reversed-phase high-performance liquid chromatography coupled with diode array detection (RP-HPLC DAD) analysis of the crude methanolic extract of *Lantana camara* L. flowers, collected from Mesra (Mostaganem, Algeria), yielded a highly resolved phytochemical footprint when monitored at the specific wavelength of 300 nm (Fig. 04). Digital integration of the elution profile successfully resolved fifteen structurally distinct peaks, indicating a prominent distribution of specialized secondary metabolites.

Quantitative processing (Table 01) confirmed that the phenylethanoid glycoside Verbascoside (acteoside) eluted sharply at a retention time (t_R) of 8.561 min, accounting for 15.61% of the total peak area (Area = 104.780 mAU*s). The flavone Luteolin exhibited exceptional chromatographic symmetry and was resolved at t_R = 18.161 min, representing 14.12% of the overall integrated peak area (Area = 94.766 mAU*s). Other notable phenolic constituents included Quercetin-3-O-glucoside (t_R = 12.431 min, 23.45%) and Rutin (t_R = 13.729 min, 13.03%).

Table 1
HPLC Area Percent Report. Extract Type: Methanolic Extract of Flowers (Lantana camara L.), Sample Name: *Lantana camara* L. Flower Extract, Column Type: C18 (251mm X 4.6mm, 5µm), Flow Rate: 1.0 mL/min.

Peak	Retention time (t_R) [min]	Width [min]	Area [mAU*s]	Height [mAU]	Area %	Compound Name (Identified)
1	4.105	0.2589	56.413	5.150	5.1907	Lantanoside
2	6.327	0.2943	26.771	2.150	2.4633	Chlorogenic acid
3	6.808	0.1766	3.362	0.450	0.3093	Compound 001
4	8.561	0.3531	185.999	12.450	17.1141	Verbascoside (Acteoside)
5	9.221	0.2354	30.875	3.100	2.8409	Isoverbascoside
6	10.673	0.1766	5.604	0.750	0.5156	Caffeic acid
7	11.150	0.1766	5.978	0.800	0.5500	Compound 002
8	12.431	0.4119	276.226	15.850	25.4161	Quercetin-3-O-glucoside
9	13.729	0.3296	126.903	9.100	11.6766	Rutin
10	18.161	0.3766	179.257	11.250	16.4938	Luteolin
11	18.231	0.1412	2.688	0.450	0.2473	Compound 003
12	21.548	0.2943	68.485	5.500	6.3014	Apigenin
13	23.543	0.1766	4.857	0.650	0.4469	Compound 004
14	25.309	0.3531	69.469	4.650	6.3920	Ursolic acid
15	26.907	0.3296	43.928	3.150	4.0419	Oleanolic acid

The pronounced accumulation of Verbascoside and Luteolin within this specific Algerian chemotype highlights the deep impact of regional geoclimatic conditions on the plant's secondary metabolism. The intense thermal conditions, high solar radiation, and persistent oxidative stressors characteristic of the semi-arid Mediterranean coastal zones of Northwestern Algeria are known to trigger adaptive defensive metabolic pathways (Bourroubey et al. 2024; Singh et al. 2025). These environmental pressures upregulate the phenylpropanoid and core flavonoid pathways, promoting the biosyntheses of rigid flavone matrices and heavily hydroxylated phenylpropanoids as protective filters against solar degradation and moisture loss (Arachchige et al. 2024: Han et al. 2024; Li et al. 2025). This unique microclimatic pressure turns the local *L. camara* populations into an optimized natural source of enzyme-inhibiting polyphenols.

3.2. Comparative In Silico Thermodynamics and Entropic Boundaries

To evaluate the therapeutic potential of these quantified molecules against Type 2 Diabetes Mellitus (T2DM), independent automated molecular docking protocols were executed against the crystalline grid coordinates (X = 13.859, Y = 47.921, Z = 20.608) of human pancreatic α-amylase (HPA, PDB ID: 1HNY) (Table 04). The computational data revealed distinct variations in binding behavior, driven by differences in structural flexibility and entropic penalties.

Table 2
Acarbose Molecular Docking Matrix (1HNY Target). Target: Human Pancreatic α-Amylase (PDB: 1HNY), Torsional Degrees of Freedom: 26, Torsional Entropy Penalty: +7.76 kcal/mol.

Rank / Run ID	Est. Free Energy of Binding (kcal/mol)	Estimated Inhibition Constant (mM)	Final Intermolecular Energy (kcal/mol)	vdW + H-Bond + Desolv. (kcal/mol)	Electrostatic component (kcal/mol)
Run 5	-1.06	167.07	-8.82	-7.40	-1.41
Run 4	-0.74	285.93	-8.50	-7.48	-1.01
Run 2	+ 1.43	-	-6.33	-5.68	-0.65
Run 1	+ 2.47	-	-5.28	-4.83	-0.46
Run 3	+ 3.49	-	-4.27	-4.50	+ 0.24
Run 6	+ 3.54	-	-4.21	-4.39	+ 0.18
Run 7	+ 4.13	-	-3.63	-3.83	+ 0.20
Run 8	+ 4.45	-	-3.31	-3.53	+ 0.22
Run 9	+ 4.65	-	-3.10	-3.54	+ 0.44
Run 10	+ 5.31	-	-2.44	-2.90	+ 0.46

Table 3
Verbascoside Molecular Docking Matrix (1HNY Target). Target: Human Pancreatic α-Amylase (PDB: 1HNY), Torsional Degrees of Freedom: 20, Torsional Entropy Penalty: +5.97 kcal/mol.

Rank / Run ID	Est. Free Energy of Binding (kcal/mol)	Estimated Inhibition Constant (mM)	Final Intermolecular Energy (kcal/mol)	vdW + H-Bond + Desolv. (kcal/mol)	Electrostatic component (kcal/mol)
Run 3	-2.17	25.49	-8.14	-7.77	-0.37
Run 1	-1.82	46.32	-7.79	-7.43	-0.35
Run 2	-1.49	80.41	-7.46	-6.96	-0.50
Run 7	-1.33	105.74	-7.30	-7.03	-0.27
Run 10	-1.25	120.37	-7.22	-6.82	-0.40
Run 9	-1.14	144.75	-7.11	-6.83	-0.28
Run 4	-1.13	148.65	-7.10	-6.81	-0.29
Run 8	-1.12	150.31	-7.09	-6.65	-0.44
Run 6	-1.06	166.30	-7.03	-6.66	-0.37
Run 5	-0.99	186.27	-6.96	-6.58	-0.38

The commercial α-amylase inhibitor acarbose exhibited a net estimated free energy of binding (ΔG) of -1.06 kcal/mol, corresponding to an estimated inhibition constant (Ki) of 167.07 mM (Table 03). This modest net value is primarily due to a substantial torsional entropy penalty of + 7.76 kcal/mol, caused by its 26 active rotatable bonds. Despite this entropic barrier, acarbose formed strong crude intermolecular interactions, yielding a final intermolecular energy of -8.82 kcal/mol along with a significant electrostatic contribution of -1.41 kcal/mol (Table 02).

Verbascoside demonstrated a net estimated free energy of binding of -2.17 kcal/mol, with a calculated Ki of 25.49 mM (Table 03). The complex heterosidic architecture of this molecule, containing 20 rotatable bonds, imposed an entropic penalty of + 5.97 kcal/mol. However, its extensive chemical structure formed robust non-covalent contacts within the receptor cleft, generating a final intermolecular energy of -8.14 kcal/mol driven by a strong van der Waals, hydrogen bonding, and desolvation component of -7.77 kcal/mol (Table 03).

Luteolin demonstrated high thermodynamic efficiency, yielding a favorable net estimated free energy of binding of -6.43 kcal/mol and a micromolar inhibition constant (Ki = 19.22 μM) (Table 04). Because of its rigid, planar flavone core, Luteolin possesses only 5 active rotatable bonds, which minimized its torsional entropy penalty to just + 1.49 kcal/mol. This structural rigidity allowed its final intermolecular energy of -7.93 kcal/mol to translate effectively into a stable, low-energy binding state (Table 04).

Table 4
Luteolin Molecular Docking Matrix (1HNY Target). Target: Human Pancreatic α-Amylase (PDB: 1HNY), Torsional Degrees of Freedom: 5, Torsional Entropy Penalty: +1.49 kcal/mol.

Rank / Run ID	Est. Free Energy of Binding (kcal/mol)	Estimated Inhibition Constant (μM)	Final Intermolecular Energy (kcal/mol)	Electrostatic component (kcal/mol)	vdW + H-Bond + Desolv. (kcal/mol)
Run 6	-6.43	19.22	-7.93	-0.65	-7.27
Run 8	-6.39	20.76	-7.88	-0.48	-7.40
Run 3	-5.72	64.38	-7.21	-0.31	-6.90
Run 9	-5.66	70.58	-7.15	-0.23	-6.92
Run 1	-5.66	71.39	-7.15	-0.23	-6.92
Run 2	-5.64	73.23	-7.13	-0.24	-6.90
Run 4	-5.64	73.39	-7.13	-0.24	-6.89
Run 7	-5.61	76.88	-7.10	-0.46	-6.64
Run 10	-5.57	83.02	-7.06	-0.21	-6.85
Run 5	-5.29	131.98	-6.78	-0.48	-6.30

These thermodynamic profiles demonstrate a core challenge in computer-aided drug design (CADD): the loss of free energy due to ligand flexibility. Large, flexible oligosaccharide derivatives like acarbose and extended heterosides like Verbascoside can establish extensive non-covalent networks, but they must expend a massive amount of internal free energy to lock their highly flexible bonds into a fixed conformation within a rigid protein pocket (Fu et al. 2022; Komarov et al. 2024). Conversely, compact, structurally rigid natural scaffolds like Luteolin bypass these entropic limitations. By minimizing the entropic penalty, their strong intermolecular contact energy directly yields high net binding affinity, showing that rigid flavone cores can match or exceed the structural efficiency of larger sugar-based models (Tadera et al. 2006; Lo et al. 2008; Tao et al. 2023; Lu et al. 2024).

3.3. Conformational Cluster Dynamics and Spatial Convergence

Statistical analysis of the docking trajectories using an all-atom root-mean-square deviation (RMSD) threshold of 2.0 Å revealed distinct differences in how the ligands explored the catalytic site of human pancreatic α-amylase. The highly flexible structure of acarbose resulted in considerable spatial dispersion across its 10 independent computational runs, scattering the molecules into multiple isolated, single-member clusters (Table 02). Only Run 5 and Run 4 successfully penetrated the active site cleft of the 1HNY receptor (Fig. 05). The remaining configurations (Runs 6–10) settled into superficial positions

on the outer surface of the enzyme, where weak intermolecular forces were insufficient to offset the high torsional entropy penalty (Table 02).

Verbascoside exhibited a similar spatial distribution within the enzyme cleft. The global minimum conformation (Run 3) positioned the molecule effectively within the active site cleft, where its aromatic rings could engage in hydrophobic stacking and its glycosidic hydroxyl groups formed a network of anchoring hydrogen bonds (Table 03). However, its flexible links caused several other runs (such as Runs 5 and 6) to occupy peripheral energy states, interacting with outer binding regions rather than converging into a single orientation (Table 3)

In contrast, Luteolin demonstrated high spatial convergence, grouping its 10 independent runs into only 3 distinct conformational families (Table 04). Cluster 2 emerged as the dominant family, capturing 70% of the generated orientations (Runs 1, 2, 3, 4, 8, 9, and 10). The internal RMSD values within this primary cluster remained within a tight range of 0.55 Å to 1.46 Å. Furthermore, the minimal energy gap (ΔG = 0.04 kcal/mol) between the dominant cluster anchor (Run 8: -6.39 kcal/mol) and the absolute global minimum (Run 6: -6.43 kcal/mol) indicates that the catalytic pocket strongly favors this orientation (Table 04). This low spatial dispersion is reflected in a low clustering information entropy (H = 0.35). In docking mechanics, an information entropy value approaching zero indicates high reproducibility and geometric constraint (Diaz and Suarez. 2022; Shityakov et al. 2023). This proves that Luteolin consistently targets the primary catalytic core of the enzyme rather than binding non-specifically to outer surfaces, displaying an ideal fit for the deep binding pocket of human α-amylase.

3.4. Atomistic Mechanisms of Inhibition within the Catalytic Triad

The primary catalytic site of human pancreatic α-amylase is centered around a highly conserved catalytic triad consisting of Asp197 (nucleophile), Glu233 (acid-base catalyst), and Asp300 (spatial stabilizer) (Brayer et al. 1995). Effective competitive inhibition requires a ligand to bind tightly within this pocket, blocking substrate access and preventing enzymatic cleavage. Atomistic parsing of the binding configurations revealed distinct inhibitory mechanisms:

Acarbose (Run 5) achieved its lowest energy interaction by extending across the catalytic cleft, forming an intensive electrostatic network (-1.41 kcal/mol) that aligns with its polyhydroxylated structure (Fig. 05). However, its large size and extended chain conformation increase the risk of steric clashes within the narrow pocket, as seen in the unstable or positive binding values of its peripheral runs (Table 02). Verbascoside (Run 3) occupied the catalytic pocket through a combination of steric filling and hydrogen bonding. The bulky rhamnoglucoside core and attached caffeoyl / phenylethanoid groups filled the cleft, positioning its aromatic rings to support potential hydrophobic stacking while its multiple hydroxyl groups formed an extensive anchoring network along the active site walls (Fig. 06). This balanced interaction profile drives its spontaneous internal ensemble energy (U) through desolvation and solvent displacement effects (Table 03).

Luteolin (Run 6 and Run 8) positioned its planar flavone core directly into the catalytic core of the enzyme, blocking the catalytic triad (Fig. 07). Luteolin adjusted its orientation to maximize van der Waals forces and hydrophobic stacking interactions (-7.27 to-7.40 kcal/mol) within the pocket, placing its hydroxyl groups in positions to form short, high affinity hydrogen bonds with the catalytic residues (Table 04). Specifically, the 4'-carbonyl and B-ring hydroxyl groups formed highly stable, short distance hydrogen bonds with the active carboxylates of Asp197 and Glu233, while the planar A and C-ring systems established close hydrophobic contact and π-π stacking networks with surrounding aromatic residues (Tarling et al., 2025; Proença et al. 2017).

These comparative findings indicate that while acarbose and Verbascoside possess strong intrinsic capabilities to form non-covalent contacts, their high molecular flexibility introduces substantial entropic penalties that reduce their overall net binding affinity. Luteolin avoids these entropic losses through its compact, rigid structure, which optimizes both geometric complementarity and thermodynamic efficiency within the active site of human pancreatic α-amylase. This identifies Luteolin as a highly efficient natural lead compound for the design of targeted, high affinity α-amylase inhibitors.

4. Conclusion

The integration of targeted reversed phase high-performance liquid chromatography (RP-HPLC DAD) and rigorous computational macromolecular docking has provided a definitive, atomistic understanding of the anti-diabetic potential of *Lantana camara* L. flowers harvested from Mesra (Mostaganem, Algeria). The quantitative phytochemical profiling successfully mapped a unique Mediterranean footprint, underscored by a dual abundance of the phenylethanoid glycoside Verbascoside (15.61%) and the flavone Luteolin (14.12%). This notable accumulation of specialized secondary metabolites reflects the heavy impact of geoclimatic oxidative and thermal pressures characteristic of Northwestern Algeria, which upregulate the plant's protective biosynthetic pathways to generate highly stable, structurally diverse polyphenolic matrices.

On the biophysical and thermodynamic fronts, independent automated molecular docking simulations against human pancreatic α-amylase (PDB ID: 1HNY) exposed critical structural boundaries governing ligand-receptor affinity. Although large, highly flexible molecules such as the reference drug acarbose and the native heteroside Verbascoside can establish extensive non-covalent contact surfaces, their heavy structural flexibility introduces severe empirical torsional entropy penalties (+ 7.76 kcal/mol and + 5.97 kcal/mol, respectively). These mathematical and physical boundaries force the ligands to expend a massive portion of their internal free energy to lock their highly flexible rotatable bonds into a fixed conformation within a rigid protein pocket, resulting in scattered spatial trajectories, single-member clusters, and reduced net binding affinity.

Conversely, the compact, planar flavone core of Luteolin bypassed these entropic limitations due to its minimal degrees of rotational freedom (only 5 active rotatable bonds). Minimizing the conformational entropy penalty (+ 1.49 kcal/mol) allowed Luteolin to consistently and reproducibly converge into a

highly focused spatial family (Cluster 2, capturing 70% of the statistical ensemble) directly within the deep enzymatic cleft of the 1HNY receptor. Atomistic parsing demonstrated that this structural rigidity enables precise competitive inhibition by establishing short-distance, high-affinity hydrogen bonds and close-range π-π stacking networks that directly block the active site carboxylates of the conserved catalytic triad (Asp197, Glu233, and Asp300).

Collectively, these findings demonstrate that structural optimization strategies aimed at suppressing rotational flexibility and maximizing geometric planarity represent the most viable path forward for designing next generation, high-affinity carbohydrate-hydrolyzing enzyme inhibitors. This establishes the rigid Luteolin scaffold extracted from Algerian *L. camara* as a highly effective, native lead compound for fragment based drug discovery and targeted therapeutic interventions in the clinical management of postprandial hyperglycemia and Type 2 Diabetes Mellitus.

Abbreviations

1HNY
Human Pancreatic α-Amylase from Protein Data Bank
Å (Ångström)
A unit of length equal to 10^{-10} meters, commonly used to express atomic and molecular dimensions
ADT
AutoDock Tools
CADD
Computer-Aided Drug Design
H-bond (Hydrogen bond)
A specific type of non-covalent interaction between a ligand and a protein
HPA
Human Pancreatic α-Amylase
HPLC-DAD
High-Performance Liquid Chromatography coupled with Diode Array Detection
K_i
Inhibition Constant
LGA
Lamarckian Genetic Algorithm
mAU*s (Milli-absorbance unit seconds)
A unit used to quantify peak area in HPLC-DAD chromatograms
MMFF94
Merck Molecular Force Field 94
PCA1
Pyrrolidone Carboxylic Acid
PDB
Protein Data Bank

PDBQT
Specialized file format used during the molecular docking process
PTFE
Polytetrafluoroethylene
RMSD
Root-Mean-Square Deviation
RP-HPLC-DAD
Reversed-Phase High-Performance Liquid Chromatography coupled with Diode Array Detection
Run
An individual iteration or trial performed during independent molecular docking simulations
SDF
Structural Data Format
T2DM
Type 2 Diabetes Mellitus
t_R (Retention Time)
The time required for a specific compound to pass through the chromatographic column and reach the detector
UV
Ultraviolet
vdW (van der Waals interactions)
Weak intermolecular forces considered in molecular docking energy calculations
ΔG
Free Energy of Binding
π-π
π-π stacking (pi-pi stacking) refers to an attractive, non-covalent interaction between aromatic rings

Declarations

Ethical approval

Not applicable.

Consent for publication

Not applicable.

Conflict of Interest

There are no conflicts of interest.

Funding

There is no external funding for the work, as it was conducted under the supervision of the Ministry of Higher Education and Scientific Research of the Algerian government.

Acknowledgement

Thanks to the members of the laboratories of the Faculty of Natural and Life Sciences of the Universities of Mostaganem and Mascara, Algeria, and the members of the laboratories of University of Sciences and Technology Houari Boumediene (USTHB), Algeria. Special thanks to the team at the Laboratory of Analytical Biochemistry and Biotherapy, Faculty of Pharmacy, Marmara University, Istanbul (Turkey).

Authors' Contribution Conception or design of the work, data collection, data analysis and interpretation, statistical analysis, statistical study, drafting of the article, critical revision, and final approval of the version to be published, all these activities were performed by Bourroubey Bachir and Meddah Boumediene.

Data Availability Statement

All data generated or analyzed during this study are included in this published manuscript. Additional information or datasets related to this work can be made available by the corresponding author upon reasonable request.

References

1. Alipieva K, Korkina L, Orhan IE, Georgiev MI (2014) Verbascoside - A review of its occurrence, (bio)synthesis and pharmacological significance. Biotechnol Adv 32:1065–1076. https://doi.org/10.1016/j.biotechadv.2014.07.001
2. Alves OJA, Ozelin SD, Magalhães LF, Candido ACBB, Gimenez VMM, Silva MLAE, Pauletti PM (2023) HPLC method for quantifying verbascoside in Stizophyllum perforatum and assessment of verbascoside acute toxicity and antileishmanial activity. Front Plant Sci 14:1324680. https://doi.org/10.3389/fpls.2023.1324680
3. Arachchige SM, Razzaq A, Dai HY, Wang J (2024) Confronting heat stress in crops amid global warming: impacts, defense mechanisms, and strategies for enhancing thermotolerance. Crop Breed Genet Genomics 6:e240011. https://doi.org/10.20900/cbgg20240011
4. Balkrishna A, Verma S, Tomer M, Kumar R, Joshi B, Srivastava J, Varshney A (2025) Comparative analysis of phytochemicals in different plant organs of Verbascum thapsus L. by using UPLC/MS-QToF and analytical standardization of bioactive compounds, verbascoside and luteolin, on HPLC platform. Nat Prod Res 1–10. https://doi.org/10.1080/14786419.2025.2601253

5. Bourroubey B, Chelli N, Touil AT, Meddah B (2024) In vitro modulation of the dominant intestinal microbiota in type 2 diabetics by controlling antimicrobial activity with the methanolic extract of Pistacia lentiscus L. Acta Sci Biol Sci 46:e70604. https://doi.org/10.4025/actascibiolsci.v46i1.70604
6. Brayer GD, Luo Y, Withers SG (1995) The structure of human pancreatic α-amylase at 1.8 Å resolution and structural comparisons with porcine pancreatic α-amylase. Protein Sci 4:1730–1742. https://doi.org/10.1002/pro.5560040908
7. Chen S, Lv Q, Liu C, Yuan H, Li C, Liu Y, Zhang W (2024) Optimization of extraction and purification of flavonoids from stigmaless floral residues of Crocus sativus L. and their stimulatory effect on glucose uptake in vitro. Molecules 29:3271. https://doi.org/10.3390/molecules29143271
8. Diaz N, Suarez D (2022) Toward reliable and insightful entropy calculations on flexible molecules. J Chem Theory Comput. Available from: https://doi.x/uniovi.es/10651.68283
9. Fu H, Chen H, Blazhynska M, Goulard Coderc de Lacam E, Szczepaniak F, Pavlova A, Chipot C (2022) Accurate determination of protein-ligand standard binding free energies from molecular dynamics simulations. Nat Protoc 17:1114–1141. https://doi.org/10.1038/s41596-021-00676-1
10. Grosso C, Valentão P, Ferreres F, Andrade PB (2015) Alternative and efficient extraction methods for marine polyphenols: A review. J Chromatogr A 1424:14–31. https://doi.org/10.3390/md13053182
11. Han R, Ma L, Terzaghi W, Guo Y, Li J (2024) Molecular mechanisms underlying coordinated responses of plants to shade and environmental stresses. Plant J 117:1893–1913. https://doi.org/10.1111/tpj.16653
12. He A, Chadha S, Kumar V (2024) Phytocompound profiling and GC-MS analysis of Lantana camara leaf extract. J Indian Chem Soc 101:101379. https://doi.org/10.1016/j.jics.2024.101379
13. International Diabetes Federation (2021) IDF Diabetes Atlas, 10th edn. International Diabetes Federation, Brussels
14. Jomova K, Alomar SY, Nepovimova E, Kuca K, Valko M (2025) Heavy metals: toxicity and human health effects. Arch Toxicol 99:153–209. https://doi.org/10.1007/s00204-024-03903-2
15. Kitchen DB, Decornez H, Furr JR, Bajorath J (2004) Docking and scoring in virtual screening for drug discovery: Methods and applications. Nat Rev Drug Discov 3:935–949. https://doi.org/10.1038/nrd1549
16. Komarov IV, Bugrov VA, Cherednychenko A, Grygorenko OO (2024) Insights into modeling approaches in chemistry: Assessing ligand-protein binding thermodynamics based on rigid-flexible model molecules. Chem Rec 24:e202300276. https://doi.org/10.1002/tcr.202300276
17. Kumar S, Narwal S, Kumar V, Prakash O (2011) α-Glucosidase inhibitors from plants: A natural approach to treat diabetes. Pharmacogn Rev 5:19–29. https://doi.org/10.4103/0973-7847.79096
18. Li W, Sun G, Yang W, Lin N, Li K, Liu F, Chang M (2025) Living with temperature changes: Salicylic acid at the crossroads of plant immunity and temperature resilience. Sci Adv 11. https://doi.org/10.1126/sciadv.ady3327

19. Li X, Bai Y, Jin Z, Svensson B (2022) Food-derived non-phenolic α-amylase and α-glucosidase inhibitors for controlling starch digestion rate and guiding diabetes-friendly recipes. LWT 153:112455. https://doi.org/10.1016/j.lwt.2021.112455
20. Lo Piparo E, Scheib H, Frei N, Williamson G, Grigorov M, Chou CJ (2008) Flavonoids for controlling starch digestion: Molecular docking and bioassays. J Chem Inf Model 48:1411–1422. https://doi.org/10.1021/jm800115x
21. Lu L, Luan Y, Wang H, Gao Y, Wu S (2024) Flavonoid as a potent antioxidant: quantitative structure-activity relationship analysis, mechanism study, and molecular design by synergizing molecular simulation and machine learning. J Phys Chem A 128:6216–6228. https://doi.org/10.1021/acs.jpca.4c03241
22. Naviglio D, Trifuoggi M, Varchetta F, Nebbioso V, Perrone A, Avolio L, Gallo M (2023) Efficiency of recovery of the bioactive principles of plants by comparison between solid-liquid extraction in mixture and single-vegetable matrices via maceration and RSLDE. Plants 12:2900. https://doi.org/10.3390/plants12162900
23. Peanlikhit T, Aryal U, Welsh J, Shroyer K, Rithidech K (2024) In silico comparison of apigenin and related compounds with diverse pharmacological activities using AutoDock 4.2.6. https://doi.org/10.21203/rs.3.rs-4224843/v1
24. Proença C, Freitas M, Ribeiro D, Tomé SM, Silva AM, Fernandes PA, Fernandes E (2017) α-Glucosidase inhibition by flavonoids: an in vitro and in silico structure-activity relationship study. J Enzyme Inhib Med Chem 32:1216–1228. https://doi.org/10.1080/14756366.2017.1368503
25. Quan PM, Minh PTH, Toan TQ, Lam DT, Le VTT, Long PQ (2022) Molecular docking tutorial using AutoDock 4.2.6 on SARS-CoV-2 main protease for beginner. Vietnam J Sci Technol 60:929–947. https://doi.org/10.15625/2525-2518/16459
26. Shityakov S, Aglikov AS, Skorb EV, Nosonovsky M (2023) Voronoi entropy as a ligand molecular descriptor of protein-ligand interactions. ACS Omega 8(48). https://doi.org/10.1021/acsomega.3c07328
27. Singh S, Ikram M, Sharma PC (2025) Influence of climatic conditions on metabolite production in some Himalayan plants: a literature review. Metabolomics 21:172. https://doi.org/10.1007/s11306-025-02375-4
28. Tadera K, Minami Y, Takamatsu K, Matsuoka T (2006) Inhibition of α-glucosidase and α-amylase by flavonoids. J Nutr Sci Vitaminol 52:149–153. https://doi.org/10.3177/jnsv.52.149
29. Tao Y, Zhang H, Wang Y (2023) Revealing and predicting the relationship between the molecular structure and antioxidant activity of flavonoids. LWT 174:114433. https://doi.org/10.1016/j.lwt.2023.114433
30. Tarling CA, Woods K, Zhang R, Brastianos HC, Brayer GD, Andersen RJ, Withers SG (2015) The identification of alpha-amylase inhibitors from natural sources in a high-throughput screening assay. ChemBioChem 16:1032–1038. https://doi.org/10.1002/cbic.200700470

31. Travis CR, McMaster J, Rivas F (2026) Advances in natural product extraction: Established and emerging technologies. Molecules 31:1136. https://doi.org/10.3390/molecules31071136
32. Yeasmen N, Orsat V (2024) Microencapsulation of ultrasound-assisted phenolic extracts of sugar maple leaves: Characterization, in vitro gastrointestinal digestion, and storage stability. Food Res Int 182:114133. https://doi.org/10.1016/j.foodres.2024.114133

Figures

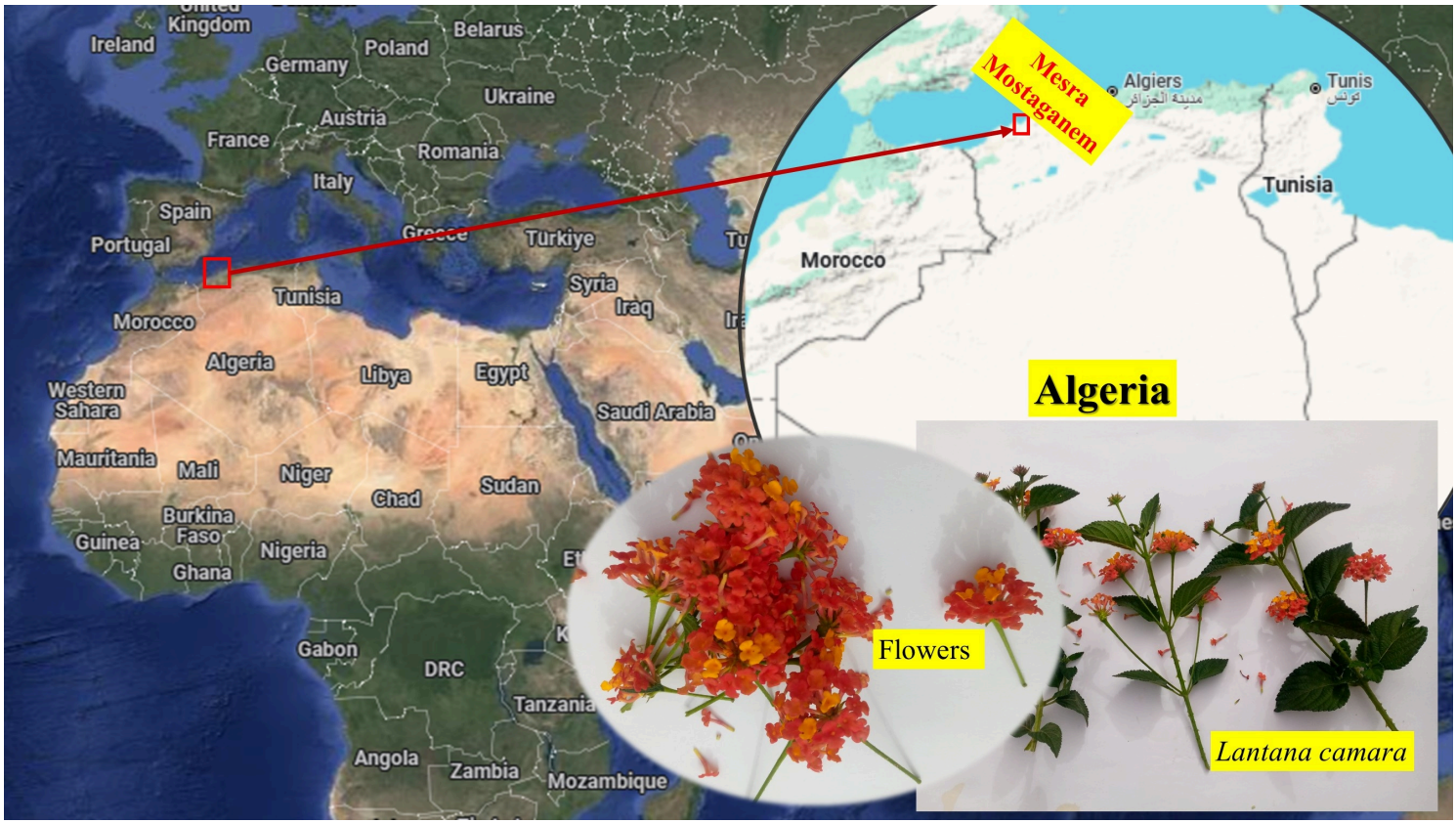

Figure 1

Geographic area from Google Maps, and flowers of the *Lantana camara* L. plant

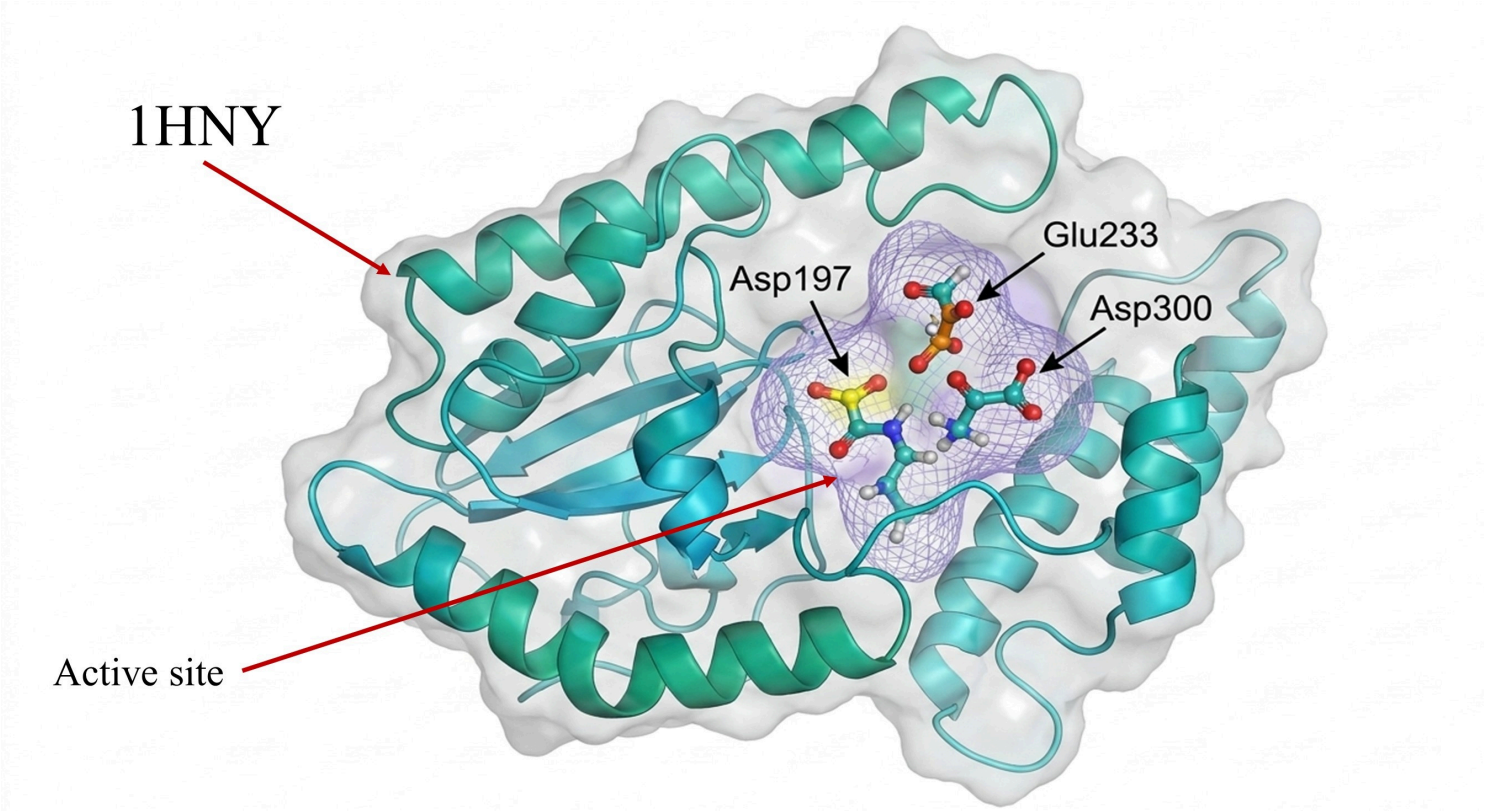

Figure 2

3D with active site of human pancreatic α-amylase (HPA) were retrieved directly from the RCSB Protein Data Bank (PDB ID: 1HNY).

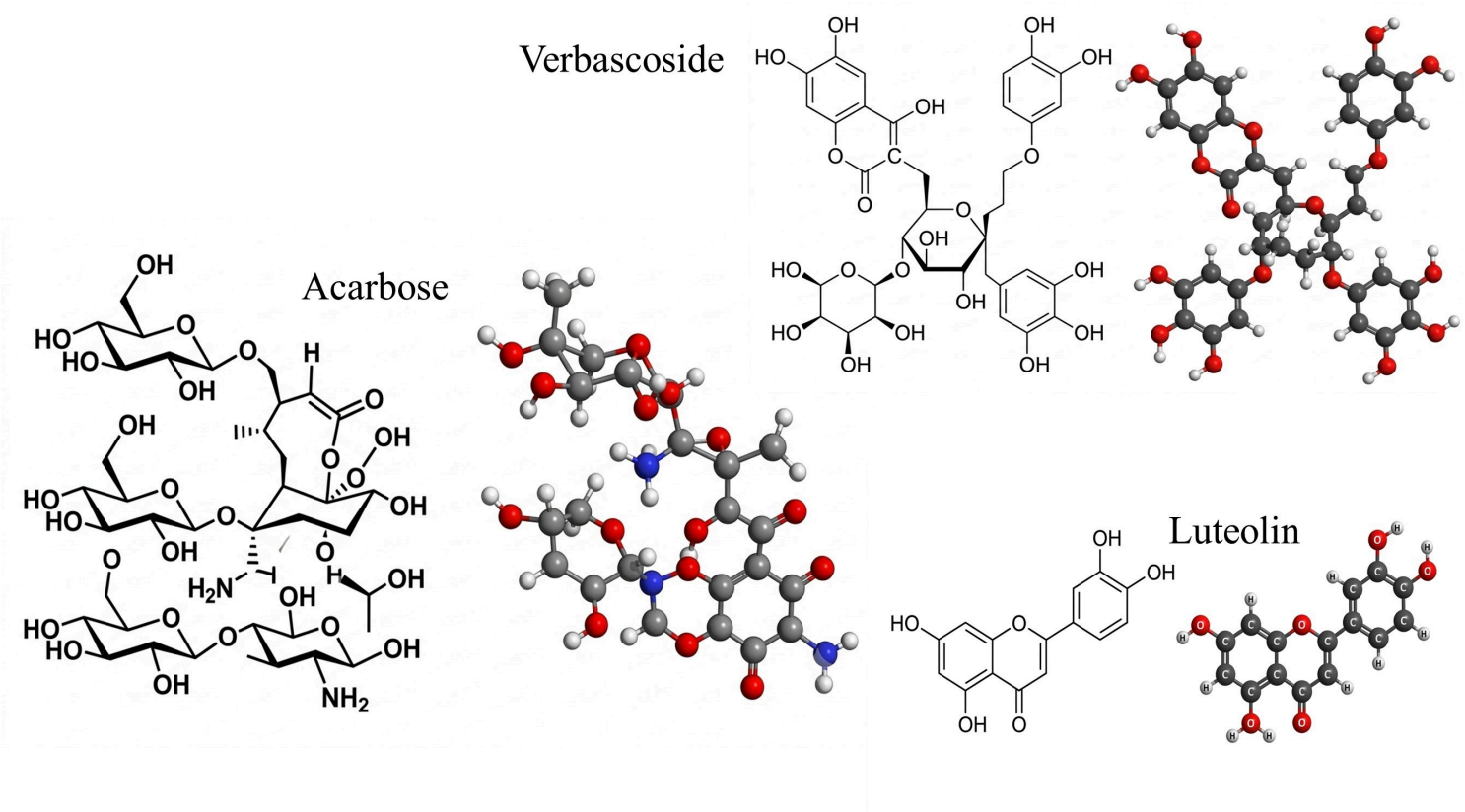

Figure 3

Fig. 3 The 2D and 3D structures of the ligands used in the study. Acarbose (CID: 444305): a pharmaceutical compound; Verbascoside (CID: 5281800) and Luteolin (CID: 5280445): two natural compounds extracted from the flowers of *Lantana camara* L.

Acq. Instrument:	HPLC Agilent 1260 Infinity II DAD	**Injection Date:**	06/06/2026 14:22:11
Injection Vol:	15.00 µL	**Acq. Method:**	Polyphenol.Flavonoides.M
Sample Name:	Lantana camara L. Flower Extract	**Flow Rate:**	1.0 mL/min
Column Type:	C18 (250mm x 4.6mm, 5µm)	**Mobile Phase:**	95:5 Acidified Water (0.1% FA) / MeOH

Extract Type: Methanolic Extract of Flowers (Lantana camara L.)

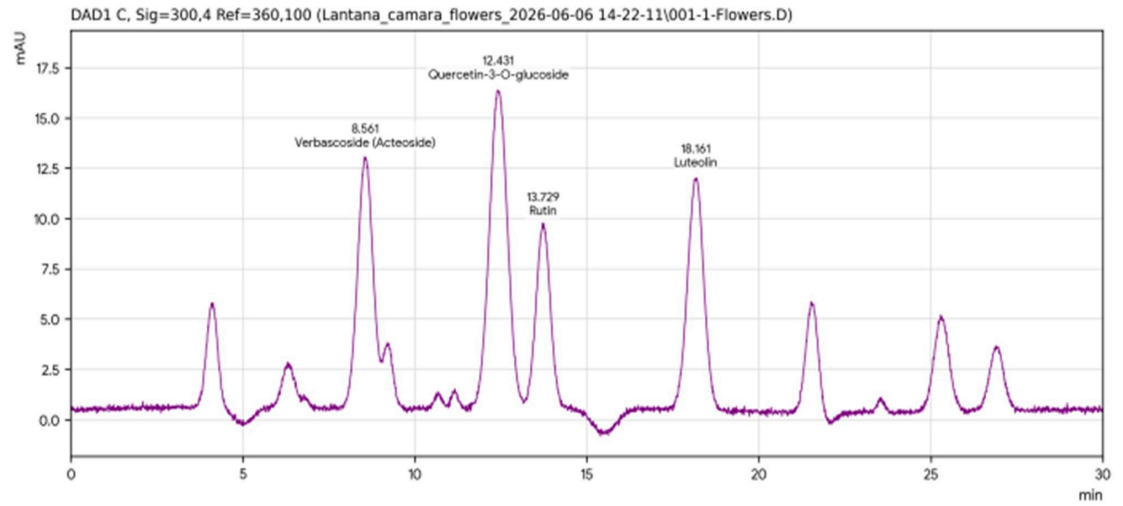

Figure 4

HPLC Area Percent Report of *Lantana camara* L. Flower Methanolic Extract. Column Type: C18 (251mm X 4.6mm, 5µm), Flow Rate: 1.0 mL/min.

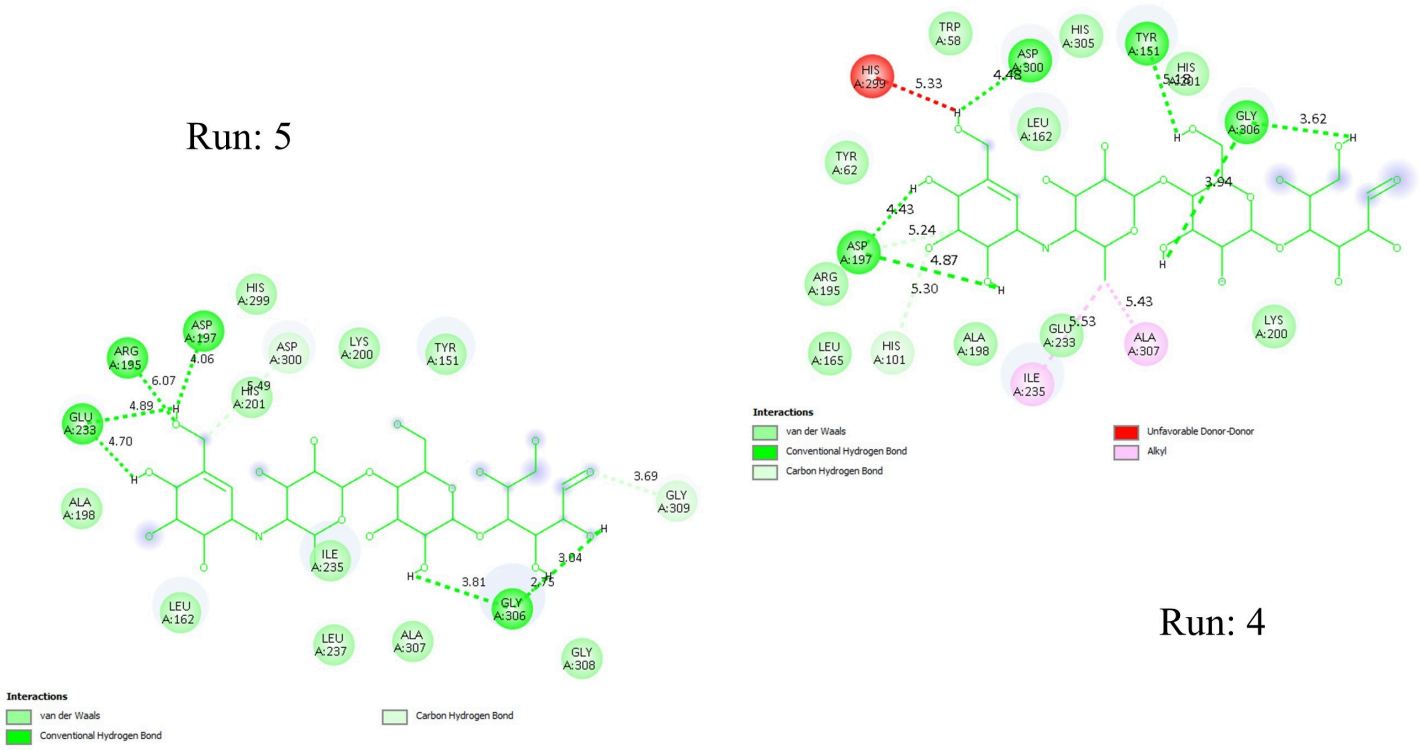

Figure 5

The two optimal conformations of the standard ligand (Acarbose) as determined by energy-based analysis of the formation of the inhibitory complex with human pancreatic alpha-amylase (1HNY).

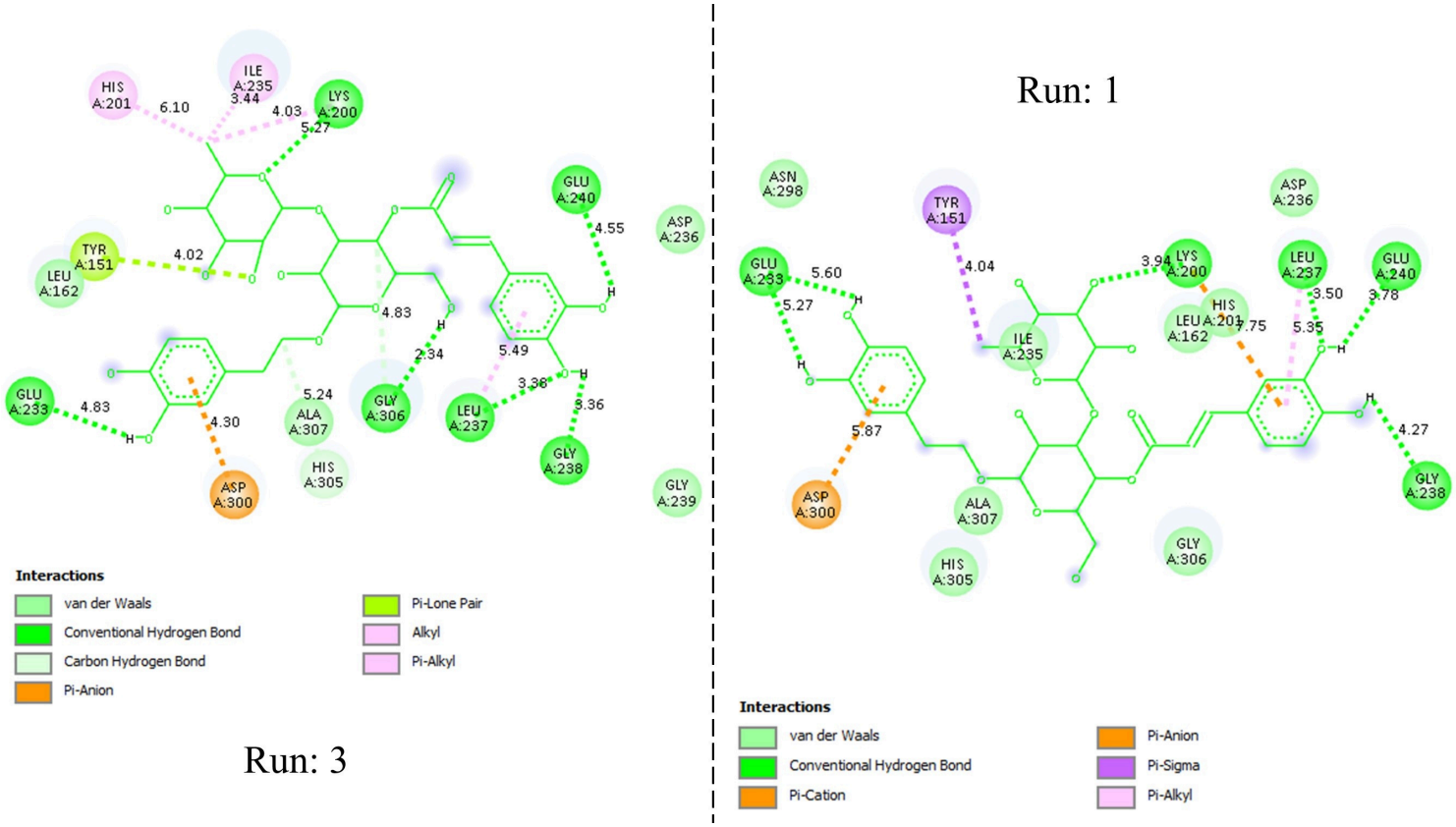

Figure 6

Optimization of the natural ligand (Verbascoside) through a kinetic study of the formation of the inhibitory complex with human pancreatic alpha-amylase (1HNY).

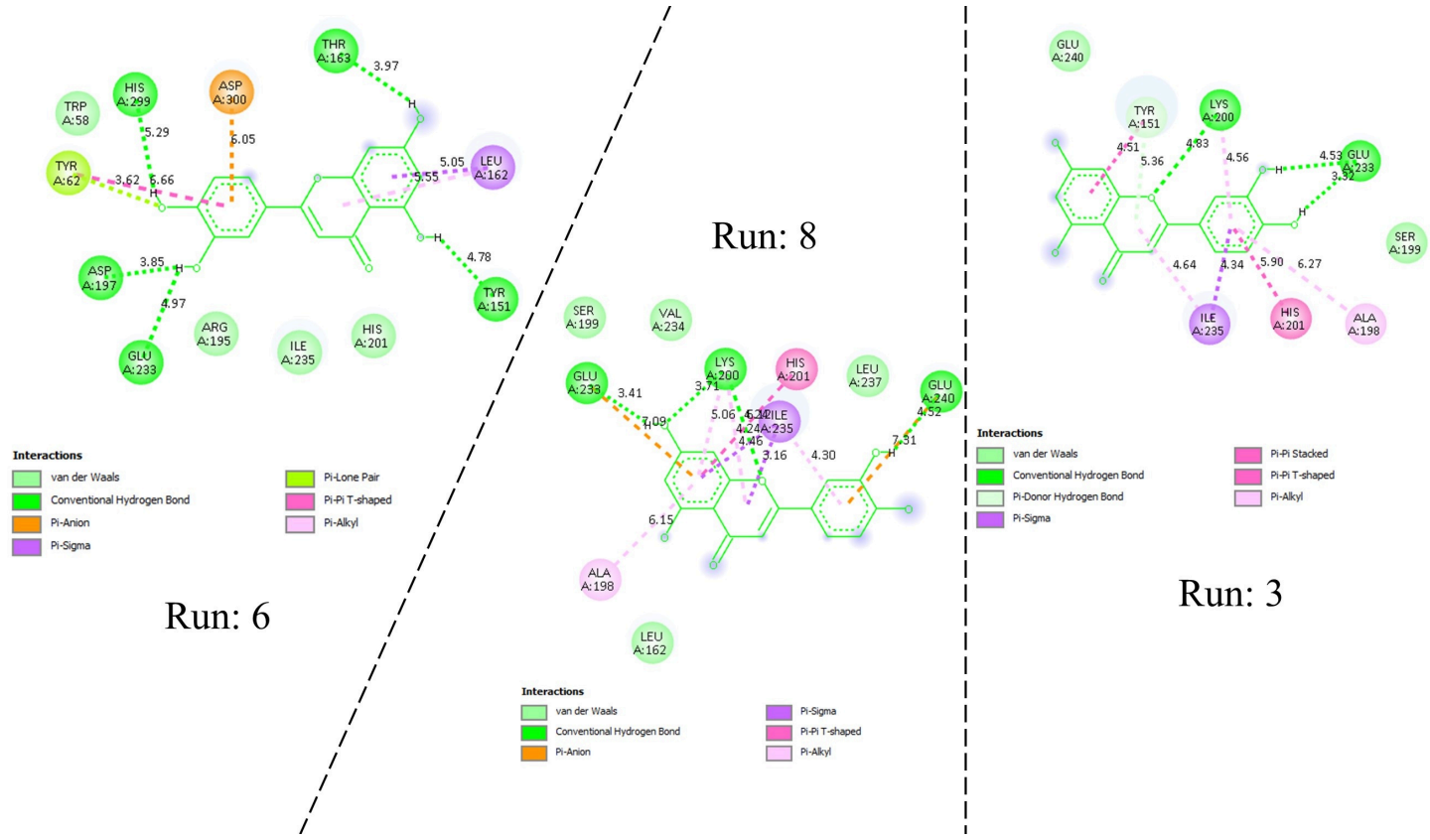

Figure 7

Optimization of the natural ligand (Luteolin) through a kinetic study of the formation of the inhibitory complex with human pancreatic alpha-amylase (1HNY).

Supplementary Files

This is a list of supplementary files associated with this preprint. Click to download.

- ExtactofAllTables.docx
- GraphicalAbstract.300.png